

# Two-dimensional constriction flows of foams

S.A. Jones<sup>a</sup>, B. Dollet<sup>b</sup>, N. Slosse<sup>c</sup>, Y. Jiang<sup>d</sup>, S.J. Cox<sup>a</sup>, F. Graner<sup>c,e</sup>

<sup>a</sup>*Institute of Mathematics and Physics, Aberystwyth University, Aberystwyth SY23 3BZ, UK*

<sup>b</sup>*Institut de Physique de Rennes, UMR CNRS 6251, Université Rennes 1, Campus de Beaulieu, Bât. 11A, CS 74205, 263, av. du Général Leclerc, 35042 Rennes Cedex, France*

<sup>c</sup>*Laboratoire de Spectrométrie Physique, UMR5588, CNRS-Université Grenoble I, BP 87, 38402 Martin d'Hères Cedex, France*

<sup>d</sup>*Theoretical Division, Los Alamos National Laboratory, Los Alamos, NM 87545, USA*

<sup>e</sup>*CNRS - Institut Curie, UMR 3215, BDD, 26 rue d'Ulm, F - 75248 Paris Cedex 05, France*

---

## Abstract

The flow of a quasi-two-dimensional foam through a constriction is described. The bubble velocity and elongation (texture) is compared between two sets of experiments and two different quasi-static simulations using Surface Evolver and Potts Model. The simulations capture the effect of changing the degree of rounding of the corners of the flow geometry and the length of the constricted region. Validation of these simulation methods offers the possibility to easily vary many parameters of interest and to explore parameter ranges that are inaccessible to experiments such as low liquid fraction and slow velocity. Perspectives include characterisations of a 3D flow at the bubble scale.

*Key words:* Surface Evolver, Potts Model, 2D constriction flow, texture tensor, quasi-2D foam

*PACS:* 83.80.Iz Emulsions and foams; 47.50.-d Non-Newtonian fluid flows

---

## 1. Introduction

Flow through a constriction, or contraction-expansion flow, is a benchmark used to establish and test rheological models of complex fluid flows such as polymer solutions [1], since it requires the fluid to submit to both shear and extensional strains. In particular, such a flow geometry allows careful comparison of the predictions of models with controlled laboratory experiments.

With their visible bubble-scale structure [2], foams are complex fluids [3] that lend themselves naturally to such a comparison. They are one of the simplest materials to exhibit behaviour that is simultaneously viscous, elastic and plastic [4, 5, 6].

A foam is discrete by nature. In principle, this would imply that its behaviour can be described only by taking into account in detail all degrees of

---

*Email address:* foams@aber.ac.uk (S.J. Cox)

freedom of the bubbles. This task is at present inaccessible to analytical treatment and can be handled only by simulations. A recurrent question is whether the foam can be described as a continuous material. This would mean that its behaviour could be understood and described by a smaller number of variables and of equations [5, 6, 7, 8], for example with fields such as velocity and stress. In this respect simulations are a crucial step to link the discrete to the continuous behaviour and the predictions of theory to experiment.

Aloui and Souhar [9, 10] were able to measure pressure drop and velocity of bubbly flows in 2D through a sudden expansion, reminiscent of extrusion flows. Deshpande and Barigou [11] studied the flow of foam past a sudden constriction or expansion in a circular pipe; they treated the foam as a continuum, measuring the effect of the change in geometry on the liquid fraction and bubble volumes. Asipauskas et al. [12] measured the velocity field and elastic stress (and later the local plasticity [6]) for a foam flowing into a 20:1 constriction in 2D; they showed that the texture tensor [12, 6] is an appropriate way to quantify the local strain in a flowing foam. Bertho et al. [13] measured bubble velocities into a similar constriction, making the link with granular materials. More recently, Dollet [14] performed a comprehensive set of experiments on quasi-2D foams flowing through a number of different constriction geometries.

Our approach aims to quantify at the bubble-scale the effect of two specific geometric features of the constriction: the degree of rounding of the corners and the length of the constricted part of the geometry. Here, we report progress on the ability of simulations to reproduce the flow of foams in two dimensions by comparing the output of two experiments and two simulation tools. Experiments consist of bubbles trapped between two parallel sheets of glass: a 2D flow of a quasi-2D foam. The quasi-2D geometry offers the advantages that each bubble’s deformation and velocity can be observed and measured straightforwardly. Simulations offer the possibility to easily vary many parameters, and to reach parameter ranges that are inaccessible to experiment. For instance, here we simulate the slow flow rate and dry foam limits (while in experiments the foam has finite velocity and liquid fraction). We expect that in this dry quasistatic limit, the foam exhibits a bubble-scale geometry dictated by Plateau’s laws: films are circular arcs (according to Laplace-Young law) which meet in threes at  $120^\circ$  angles [2, 4].

## 2. Methods

The shape of the constriction is specified by three parameters – see figure 1 – each normalized by the width of the channel  $W$ : the constriction width  $c_w/W$ , the constriction length  $c_l/W$  and the rounding of the corners  $\varepsilon/W$ . The constriction ratio is therefore  $c_r = 1 - 2c_w/W$ . Other parameters are the mean bubble area  $A_b$  and, in the experiments, the flow-rate  $Q$  and plate separation  $h$ .

To describe the foam flow and effect the comparisons between experiments and simulations, we use quantitative statistical tools. They are measured on one image or on the difference between two successive images (kinematical tools), as averages over rectangular subregions (“boxes”) of the foam channel and over

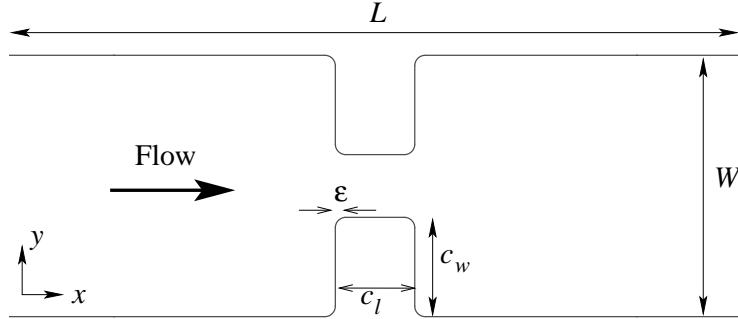


Figure 1: Geometrical parameters of the constriction flow. The width of the channel is  $W$  and the width of the constriction is measured by  $c_w$ .

time, that is, successive images in steady flow. Here we compare (i) the velocity  $\underline{v} = (v_x, v_y)$  of the bubbles, averaged over time, normalized by the value at the centre of the inflow region, denoted  $v_0$ ; (ii) the texture tensor  $\underline{M}$  [12, 6], which is symmetric and can therefore be represented by an ellipse; we also show its normalized extensional component

$$M_n = \frac{M_{xx} - M_{yy}}{M_{xx} + M_{yy}}, \quad (1)$$

which measures the stretching of the bubbles.

### 2.1. Experiment type A

A Hele-Shaw cell of length  $L = 70$  cm and plate separation  $h = 1.5$  mm was constructed by cutting constriction profiles from 1.5 mm thick PTFE sheet and sandwiching them between two horizontal glass plates. The channel width is  $W = 12$  cm,  $c_l = 3$  cm, and a constriction ratio of 0.25 was obtained by setting  $c_w = 4.5$  cm.

The foaming solution used was 2.5% Fairy liquid in de-ionised water. A foam was created by blowing compressed air through a nozzle, and the over-pressure generated created the driving force for the foam flow along the Hele-Shaw cell. The volumetric flow rate was  $Q = 0.39$  ml s<sup>-1</sup> and the average bubble area was  $0.096 \pm 0.026$  cm<sup>2</sup>. We estimated the liquid fraction, [by weighing the liquid emerging from the end of the channel](#), to be  $\phi_l \approx 0.005$ . The Hele-Shaw cell was backlit to give good contrast, and the motion of the foam was recorded using a digital video camera running at 30 fps. A typical image of the foam flow is given in figure 2(a).

Data analysis was carried out using the ImageJ package with added morphology and particle tracking plugins [15]. Having identified bubble centres, “particle tracking” gave bubble velocities, and a Delauney triangulation was used to calculate the texture tensor. The data given below was averaged over 4000 frames [and over boxes with side-length 0.40](#) cm.

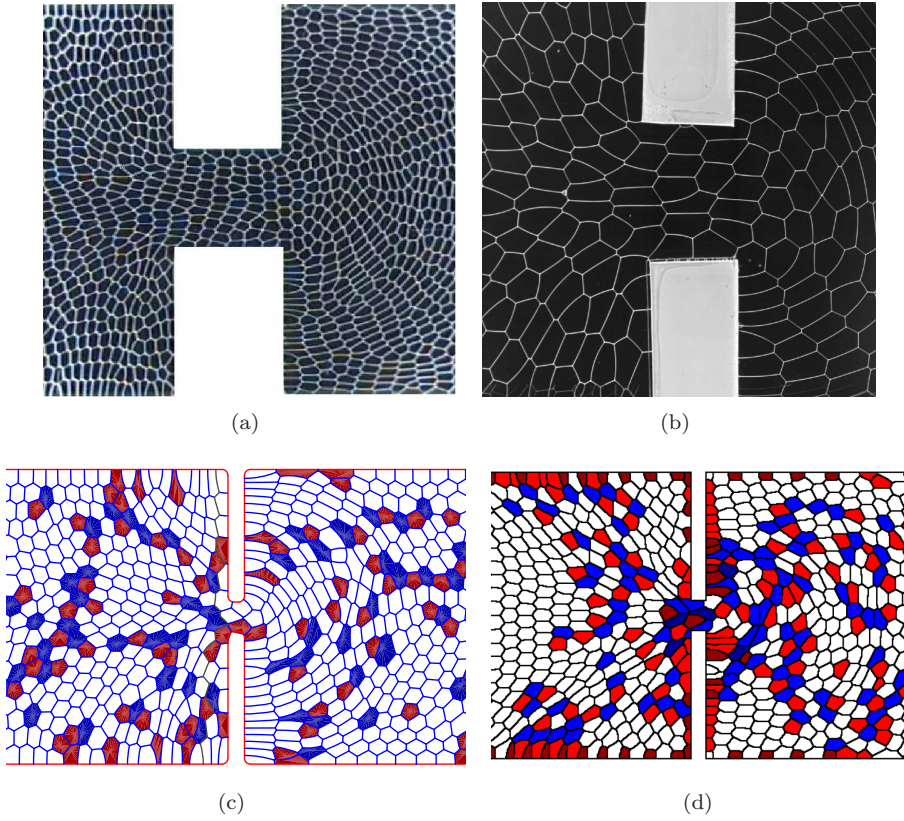


Figure 2: Images of foams with flow from left to right. (a) Type A experiment. (b) Type B experiment. (c) Surface Evolver (SE) simulations: bubbles coloured by their number of sides; owing to the periodic boundary conditions, the bubbles exiting on the right re-enter on the left. (d) Potts simulations, for the same geometrical parameters, with the same colour code. In contrast to SE, the foam is initially ordered, and the flow through the constriction creates defects. The boundary conditions are again periodic. In both (c) and (d) the periodicity is not apparent since the channel is longer than what is displayed.

## 2.2. Experiment type B

We use a setup fully described in [14] and shown in figure 2(b). Briefly, a dry foam (liquid fraction  $0.002 \leq \phi_l \leq 0.004$ ) made of nitrogen bubbles in a SDS solution (10 g/l) in ultrapure water flows in a Hele-Shaw channel of gap  $h = 2$  mm, which is small enough that the bubbles arrange in a monolayer. The length of the channel is  $L \approx 75$  cm, its width is  $W = 19.2$  cm, and the width of the constriction is  $c_w = 3.2$  cm. In this paper, we revisit three of the experiments presented in [14], with a varying constriction length:  $c_l = 2$  (see figure 2(b)),  $c_l = 5$  and  $c_l = 15$  cm; the flow rate is 2.5, 2.5 and 7.5 ml s<sup>-1</sup>, and the mean bubble area is 39, 33 and 34 mm<sup>2</sup>, respectively. Polydispersity is about 20%.

The movies of the flow (1000 images at 50 fps) are analysed by home-made image analysis [14]: the foam is skeletonised, and the motion of each bubble tracked between consecutive frames, as well as the network of neighbouring bubbles used for texture calculation. The fields describing the foam flow are computed over [boxes with side-length 0.64 cm](#).

## 2.3. Simulation: Surface Evolver (SE)

We use the Surface Evolver [16] to perform a quasi-static simulation of a disordered monodisperse foam flowing through the constriction. Each film is represented as a circular arc and the foams have 704 or 725 bubbles in a channel of length  $L = 1$  and width  $W = 0.5$ . There are free-slip boundary conditions on the channel walls, and bubbles going out at the right re-enter on the left (periodic boundary conditions) – see the example in figure 2(c). Flow is achieved by choosing a line of films that span the channel and, at each iteration, moving them downstream [a distance  \$\approx 5 \times 10^{-4}\$](#)  [17] before finding a minimum of surface energy (total perimeter). We chose a cut-off length for topological changes,  [\$l\_c = 0.001\$](#) , appropriate to simulate the effect of a liquid fraction of  $10^{-5}$  [17].

We calculate the centre of each bubble as an average of its vertex positions, so that in this way the displacement between iterations (velocity) and instantaneous texture tensor can be found. We assume that the flow is steady and average the data over 1000 iterations [and over boxes with side-length 0.017](#).

## 2.4. Simulation: Potts Model

Potts model simulations of foam flow minimize the same energy as the SE, and with the same boundary conditions, but stochastically (Monte Carlo). This increases the simulation speed and allows the simulation of a larger number of bubbles: [in SE the total simulation time is about two weeks while the Potts simulations described here take only about two hours](#).

The method is described in detail elsewhere [17]. Briefly, in a channel of  $1000 \times 200$  pixels, with a constriction of  $10 \times 20$  pixels, each bubble is defined as a connected set of pixels on a square lattice (as in experimental pictures). Thus, bubbles tile the plane without gaps or overlaps; an example is shown in figure 2(d). The energy  $H$  has three contributions: an interface cost between bubbles, with line tension  $\lambda = 3$ ; an area conservation term, with a bubble target area

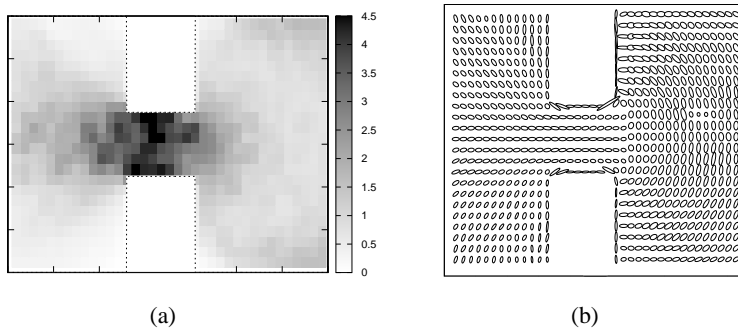


Figure 3: Fields for the experiment of type A with sharp corners: (a) velocity magnitude  $|v|/v_0$  and (b) texture, shown as ellipses [6] demonstrating the direction and magnitude of the local strain.

of 100 pixels and bubble compressibility  $\chi = 2$ ; and an external forcing of the flow with bias equal to 1.1. The bias is chosen as the minimal value necessary to overcome the pressure drop across the constriction, so that the flow is nearly quasistatic; it is a constant across the simulation domain in any given simulation, but must be recalculated for different constriction parameters. At each Monte Carlo step, each pixel is visited once on average: its value is changed to that of a neighbouring bubble (thus effectively moving the boundary between bubbles) if and only if it decreases the total foam energy. A simulation is performed in  $10^5$  to  $5 \times 10^5$  Monte Carlo steps. Measurements are performed over all successive images once the steady state is reached, using  $20 \times 20$  pixel boxes.

### 3. Results

Fields of velocity magnitude and texture are shown in figure 3 for the experiment of type A. We observe a wedge of low velocity near each upstream corner, with almost no motion in the corners themselves, and a half-annulus of low velocity downstream of the constriction. The texture shows that bubbles upstream are stretched towards the constriction, and then perpendicular to it downstream. These fields are broadly similar for all experiments and simulations; we therefore don't show them in the other cases, and instead make a more quantitative comparison of the values along the centreline of the flow.

#### 3.1. Rounded corners

We use two values of the corner curvature to compare the experiment of type A with the SE simulations. First, a *rounded* corner, with a large value of  $\varepsilon/W = 0.04$ . Second, a *sharp* corner, with a value of  $\varepsilon/W$  as small as possible: less than  $10^{-3}$  in experiment and  $\varepsilon/W = 0.01$  in the SE simulation, which requires the gradient of the energy to be continuous so that it is not possible to

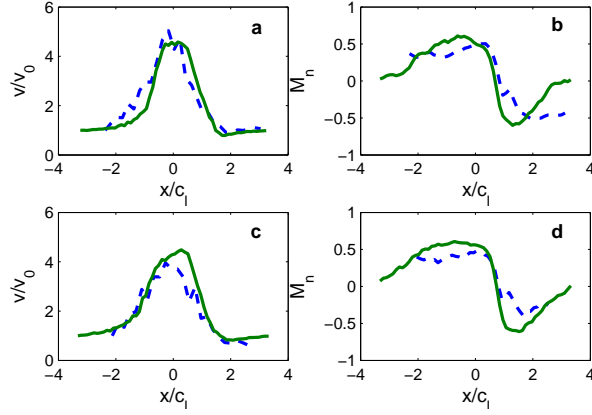


Figure 4: Effect of corner sharpness on velocity and texture, comparing Type A experiment (dashed lines) and SE simulation (solid lines). (a) Rescaled stream-wise velocity  $v_x/v_0$  on centreline for rounded corners. (b) Texture  $M_n$  on centreline for rounded corners. (c) and (d) Same for square corners. The range of  $x$  corresponds to the limit of the SE simulation.

**simulate sharp corners.** Recall that the constriction dimensions are  $c_l/W = 0.25$  and  $c_w/W = 0.375$ .

The streamwise velocity  $v_x$  on the centreline in each case is shown in figure 4.  $v_x$  rises from its free-stream value  $v_0$  to a plateau, the length of which depends upon the constriction length  $c_l$ . The velocity then decreases smoothly into the velocity trough at the constriction exit before returning back to  $v_0$ . The simulation with square corners has a less symmetrical plateau than that for the rounded corners, and also exhibits a more gradual rise in velocity so that the effect of the constriction is observed much further upstream with square corners than with rounded corners.

The agreement between experiment and simulation is good in general, with the best agreement being found for the square constriction. The slower rise in the simulated velocity upstream of the constriction **in the case of sharp corners** gives a much better prediction of the actual behaviour of the flow, with the location and slope of the increase and decrease in velocity agreeing well. The biggest discrepancy between the simulations and experiments is in the length of the plateau region, with the experimentally-measured velocity starting to drop significantly before the simulations predict that it will.

The texture  $M_n$  increases from zero far upstream, indicating isotropy, drops rapidly in the constriction, and then increases back towards zero, although the regions of isotropy lie beyond the region shown. One failing of the SE simulation becomes apparent:  $M_n$  certainly passes through zero, but the channel is too short to show a plateau in  $M_n$ ; instead it is the periodic boundary conditions that impose that  $M_n$  has to increase again to return to its upstream value. Nonetheless, close to the constriction the prediction of the position at which  $M_n$  decreases and its slope is good.

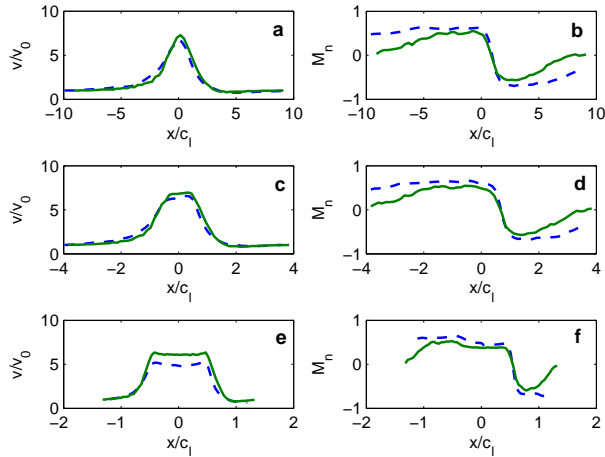


Figure 5: Effect of constriction length on velocity and texture, comparing experiment (Type B, dashed lines) and SE simulation (solid lines). (a), (c), (e) Rescaled stream-wise velocity  $v_x/v_0$  on centreline for increasing constriction length. (b), (d), (f) Texture  $M_n$  on centreline for increasing constriction length.

### 3.2. Constriction length

In this case we fix the constriction ratio, taking  $c_w/W = 0.42$ , and choose three different values of the constriction length to compare type B experiments with SE simulations: (i)  $c_l/W = 0.11$ ; (ii)  $c_l/W = 0.26$ ; and (iii)  $c_l/W = 0.78$ . In the SE simulations, the corner rounding is fixed to be  $\varepsilon/W = 0.02$ ; in the experiments it is clearly small but not measured.

The velocity on the centreline (figure 5) compares well: the magnitude is slightly overestimated by the simulation, which can be attributed to the absence of dissipation, but both show the same slope and the slight overshoot in velocity when entering and exiting the constriction. Close to the constriction the prediction of texture is again slightly overestimated compared to the experiment, which can be attributed to the higher liquid fraction in the experiment, but the position and slope where  $M_n$  drops rapidly is successfully resolved.

### 3.3. Surface Evolver vs. Potts Model

Here we choose one geometry with  $c_w/W = 0.45$  and  $c_l/W = 0.06$ ; this is a very short, thin constriction section. In SE we take  $\varepsilon/W = 0.02$ , while in Potts Model the corners [have a precision of one pixel, corresponding to  \$\varepsilon/W = 0.005\$](#) .

Streamwise velocity and texture  $M_n$  on the centreline are shown in figure 6. In both cases, the return to the free-stream values is much slower in Potts. Note that averaging effects are stronger in Potts, due to the coarser grid on which the velocity is averaged.

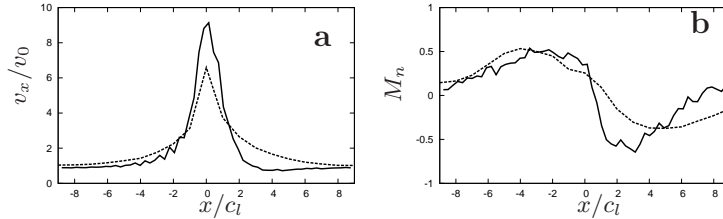


Figure 6: Comparison of SE (solid lines) and Potts Model (dashed lines) simulations. (a) Rescaled stream-wise velocity  $v_x/v_0$  on centreline. (b) Texture  $M_n$  on centreline.

#### 4. Discussion and perspectives

Since the bubbles are fairly incompressible, many of the details of a flow such as those described here can be attributed to conservation of volume, and are thus too generic to be discriminant. On the other hand, details of the chemistry of the solution used to create the foam can contribute to specific effects, which the simulations fail to take into account. In between these limits, Surface Evolver simulations capture many discriminant effects that are independent of material parameters and not wholly dictated by geometry. This includes for example both velocity overshoots, at the entrance and exit to the constriction (figure 5e); and the slope of the texture in the exit region (figure 4).

Because the Potts model can simulate many more bubbles than SE, the results from the Potts model are much less noisy. This encourages our attempts to use the Potts model to simulate 3D foam flows. Figure 7a shows the velocity field from a preliminary simulation of 3D constriction flow using the Potts model. Detailed experimental measurements of 3D foam structures are now appearing thanks to X-ray tomography [18] (figure 7b) and possibly by MRI [19], so that the comparison between experiment and simulation for 3D flow may soon become possible.

In this slow-flow limit, the effects of inertia should be negligible; the features of the flow result therefore from the subtle interplay between elasticity, plasticity and dissipation [8]. In the future, we can further validate simulations by comparing fields such as pressure and plasticity (T1s) in simulations and experiments; this would be a benchmark to test tensorial continuum models [5, 7] and their predictions of the flow, as in [8].

#### Acknowledgements

SAJ and SJC acknowledge useful discussions with D. Binding. SAJ thanks D. Francis for technical assistance. NS, YJ and FG thank C. Raufaste for providing code and assistance with the Potts Model calculation. We thank J. Lambert and P. Cloetens for permission to use figure 7b. Financial support from EPSRC/P&G grant EP/F000049/1 (SAJ, SJC), EPSRC grant EP/D071127/1

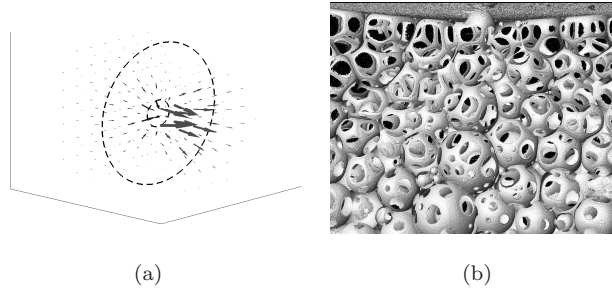


Figure 7: Axisymmetric constriction flow of a foam in three dimensions: circular hole in a cylindrical channel. (a) Velocity field in a 3D Potts simulation, with flow from left to right. (b) Wet foam experiment in X-ray tomography, showing bubbles flowing upwards into the constriction; unpublished image, 3D acquisition by J. Lambert et al., 3D rendering by P. Cloetens (ESRF).

(SJC), and the British Council Alliance Scheme (BD, SJC) is gratefully acknowledged. YJ is supported by the U.S. Department of Energy at Los Alamos National Laboratory under contract No. DE-AC52-06NA25396.

## References

- [1] D.M. Binding and K. Walters. On the use of flow through a contraction in estimating the extensional viscosity of mobile polymer solutions. *J. Non-Newtonian Fluid Mech.*, **30**:233–250, 1988.
- [2] D. Weaire and S. Hutzler. *The Physics of Foams*. Clarendon Press, Oxford, 1999.
- [3] R. Höhler and S. Cohen-Addad. Rheology of liquid foam. *J. Phys.: Condens. Matter*, **17**:R1041–R1069, 2005.
- [4] I. Cantat, S. Cohen-Addad, F. Elias, F. Graner, R. Höhler, O. Pitois, F. Rouyer, and A. Saint-Jalmes. *Les mousses - structure et dynamique*. Belin, Paris, 2010.
- [5] S. Bénito, C.-H. Bruneau, T. Colin, C. Gay, and F. Molino. An elasto-visco-plastic model for immortal foams or emulsions. *Eur. Phys. J. E*, **25**: 225–251, 2008.
- [6] P. Marmottant, C. Raufaste, and F. Graner. Discrete rearranging disordered patterns, part II: 2D plasticity, elasticity and flow of a foam. *Eur. Phys. J. E*, **25**:371–384, 2008.
- [7] P. Saramito. A new constitutive equation for elastoviscoplastic fluid flows. *J. Non-Newtonian Fluid Mech.*, **145**:1–14, 2007.

- [8] I. Cheddadi, P. Saramito, B. Dollet, C. Raufaste, and F. Graner. Understanding and predicting viscous, elastic, plastic flows. *Eur. Phys. J. E*, **submitted**:-, 2010.
- [9] F. Aloui and M. Souhar. Experimental Study of a Two-Phase Bubbly Flow in a Flat Duct Symmetric Sudden Expansion – Part I: Visualization, Pressure and Void Fraction. *Intl. J. Multiphase Flow*, **22**:651–665, 1996.
- [10] F. Aloui and M. Souhar. Experimental Study of a Two-Phase Bubbly Flow in a Flat Duct Symmetric Sudden Expansion – Part II: Liquid and Bubble Velocities, Bubble Sizes. *Intl. J. Multiphase Flow*, **22**:849–861, 1996.
- [11] N.S. Deshpande and M. Barigou. Foam flow phenomena in sudden expansions and contractions. *Intl. J. Multiphase Flow*, **27**:1463–1477, 2001.
- [12] M. Asipauskas, M. Aubouy, J.A. Glazier, F. Graner, and Y. Jiang. A texture tensor to quantify deformations: the example of two-dimensional flowing foams. *Granular Matter*, **5**:71–74, 2003.
- [13] Y. Bertho, C. Becco, and N. Vandewalle. Dense bubble flow in a silo: An unusual flow of a dispersed medium. *Phys. Rev. E*, **73**:056309, 2006.
- [14] B. Dollet. Local description of the two-dimensional flow of foam through a contraction. *J. Rheol.*, **54**:741–760, 2010.
- [15] W.S. Rasband. *ImageJ*. U.S. National Institutes of Health, Bethesda, Maryland, USA, 1997–2007. <http://rsb.info.nih.gov/ij/>. Morphology plugin from <http://www.dentistry.bham.ac.uk/landinig/software/software.html>. Particle tracking plugin from <http://valelab.ucsf.edu/~nico/IJplugins/MTrack2.html>.
- [16] K. Brakke. The Surface Evolver. *Exp. Math.*, **1**:141–165, 1992.
- [17] C. Raufaste, B. Dollet, S. Cox, Y. Jiang, and F. Graner. Yield drag in a two-dimensional foam flow around a circular obstacle: Effect of liquid fraction. *Eur. Phys. J. E*, **23**:217–228, 2007.
- [18] J. Lambert, I. Cantat, R. Delannay, A. Renault, F. Graner, J.A. Glazier, I. Veretennikov, and P. Cloetens. Extraction of relevant physical parameters from 3D images of foams obtained by X-ray tomography. *Colloids Surf. A*, **263**:295–302, 2005.
- [19] S. Rodts, J. Boujlel, B. Rabideau, G. Ovarlez, N. Roussel, P. Moucheront, C. Lanos, F. Bertrand, and P. Coussot. Solid-liquid transition and rejuvenation similarities in complex flows of thixotropic materials studied by NMR and MRI. *Phys. Rev. E*, **81**:021402, 2010.